Effect of pressure on the crystal structure of ettringite

S.M. Clark [a,*], B. Colas [a], M. Kunz [a], S. Speziale [b], P.J.M. Monteiro [c]

[a] Advanced Light Source, Lawrence Berkeley National Laboratory, 1 Cyclotron Road, Berkeley, CA 94720, USA
[b] GeoForschungsZentrum Potsdam, GeoForschungsZentrum Potsdam, Division 4.1, Telegrafenberg, 9, Potsdam, 14473, Germany
[c] University of California, Berkeley, Department of Civil and Environmental Engineering, 725 Davis Hall, University of California, CA 94720, USA

Abstract

X-ray diffraction and infrared data have been collected from a sample of ettringite from ambient pressure to 6.4 GPa. The sample was found to reversibly transform to an amorphous phase at 3 GPa. The isothermal bulk modulus of ettringite was found to be 27(7) GPa and the incompressibilities of the lattice parameters were found to be 71(30) GPa along a and 108(36) GPa along c.
Published by Elsevier Ltd.

Keywords: Amorphous material; Crystal structure; X-ray diffraction; Ettringite

1. Introduction

Ettringite is a hydrated calcium aluminum sulfate hydroxide $(Ca_6Al_2(SO_4)_3(OH)_{12} \cdot 26H_2O)$. It is a mineral that rarely occurs in nature but is an important hydration product of portland cement, formed from the reaction of calcium aluminate with calcium sulfate, affecting both short term strength development [1] and long term stability [2,3]. The formation of secondary ettringite is associated with the expansion and degradation of concrete exposed to sulfate attack [4]. The crystal structure of ettringite is known [5–8]. It is composed of columns of $Ca_6[Al_2 (OH)_{12} \cdot 24H_2O]^{6+}$ lying parallel to the c-axis with sulfate and water molecules in the inter-column channels joining the whole structure together by a network of hydrogen bonds (Fig. 1). The structure is quite open with a large proportion of interconnected void space allowing some mobility of water and hydrated ions. The ettringite structure is quite flexible allowing interchange of atomic species. It forms a partial solid solution with thaumasite [9] and has potential applications in waste management [10].

The thermal dehydration of ettringite has been studied [11–14] with some disagreement over the exact order of hydroxyl and free water leaving the crystal but general agreement over a large water loss at 110 °C followed by amorphization of the sample after the loss of 20 water units.

Given that 80% of the atoms in this mineral are either part of a water molecule or a hydroxide, resulting in a specific gravity of 1.7 one could regard ettringite as being almost all water and as such might expect it to be an extremely soft solid and
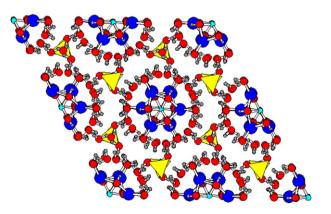

Fig. 1. Crystal structure of ettringite projected on to the (0001) plane [6]. $Ca_6[Al_2(OH)_{12} \cdot 24H_2O]^{6+}$ columns lie parallel to the c-axis with sulfate and water molecules in the inter-column channels. Ca atoms are displayed as blue circles, oxygen atoms in red, aluminum atoms in light blue, sulfate tetrahedral in yellow and hydrogen atoms in grey.

* Corresponding author.
  E-mail address: smclark@lbl.gov (S.M. Clark).

potentially unstable under compression. Here we report the results of an X-ray and infrared study of the effect of pressure on the crystal structure of ettringite. Although the pressures that our ettringite sample was subjected to in this study are much higher than could exist in a cement paste this approach to studying the stability of cement phases is important since it gives us insight into the underlying factors controlling phase stability and helps us understand the possible mechanisms controlling reactivity by analogy to simpler systems.

2. Experimental

The samples investigated in this study were obtained from a natural sample of ettringite from N'Chwanning mine, Kurruman, South Africa [15]. The sample was characterized at the GeoForschungsZentrum in Potsdam by energy-dispersive elemental analysis (EDX), infrared absorption spectroscopy and powder X-ray diffraction. The EDX analysis was carried out using a Zeiss DSM 962 operated at 20 kV, 0.55 μA. We did not detect the presence of Si within EDX analytical resolution (Table 1), in addition we did not observe the typical infrared absorption bands for $[Si(OH)_6]^{2-}$. Also, the low intensity of the absorption band of $[CO_3]^{2-}$ compared with existing data for the ettringite end member [9] confirms that our sample correspond to almost pure ettringite. The measured unit cell parameters are $a_0 = 11.240 \pm 0.001$ Å, $c_0 = 21.468 \pm 0.006$ Å, in good agreement with values from the literature [5,6]. For our experiments we selected a transparent, prismatic fragment 5 mm long and 2 mm wide from a larger specimen and ground to it to a fine powder of about 5 μm particle size.

High-pressures were generated using diamond anvil cells (dacs). Typical features of a dac are shown in Fig. 2. Samples are contained between two opposed diamonds. A thin metal foil is pressed between the diamonds and a hole drilled in the center to give a sample chamber. The sample together with a few chips of ruby, which are used to determine pressure, and a pressure transmitting fluid are loaded into the hole in the gasket. Pressing the diamonds together decreases the sample chamber volume and increases the pressure.

Pressure volume data were obtained by powder X-ray diffraction at beamline 12.2.2 at the Advanced Light Source (ALS). This beamline benefits from hard x-radiation generated by a superbend magnet. The beamline operates in angle dispersive geometry (monochromatic) and is equipped with an image plate detector and suitable collimation and goniometry for powder
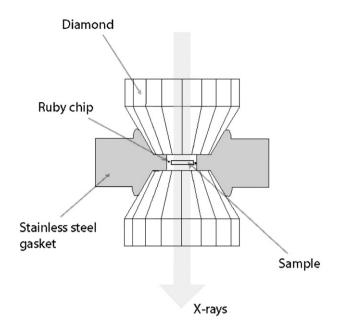

Fig. 2. Schematic diagram of a diamond anvil cell.

diffraction measurements from samples held in diamond anvil cells [16]. Data were collected using X-radiation of 15 keV energy (wavelength $\lambda = 0.82653$ Å). The beam size at the sample was set at 20×20 μm^2 in order to ensure that no diffraction from the gasket material contaminated our diffraction patterns. Any scatter from our focusing optics was removed using 100 μm Ta cleanup pinhole positioned about 60 mm in front of the diamond anvil cell. Exposure times of 300 s were found to be sufficient to give powder diffraction patterns of adequate signal to noise ratio. Powder diffraction data were collected at a total of 14 pressure points in two separate runs. For both runs, a small amount of the powdered ettringite sample was loaded into a 250 μm hole in a
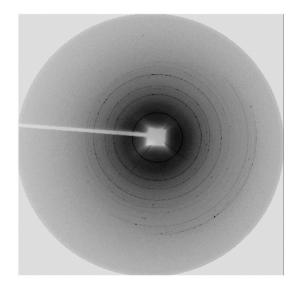

Fig. 3. Raw 2-dimensional powder diffraction pattern from an ettringite sample contained in a diamond anvil cell at ambient pressure prior to reduction to a 1-dimensional pattern using the fit2d [18] program.

Table 1
Results of EDX elemental analysis of the ettringite sample showing no detectable amount of Si to be present

Element	Atoms per formula *
Ca	6.1 ± 0.2
Si	n.d.
Al	1.7 ± 0.1
S	3.3 ± 0.1

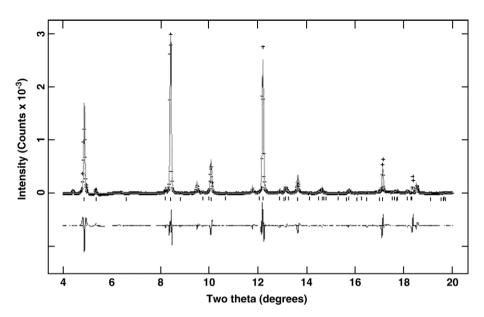* Formula based on Si + Al + Ca + S = 11.

Fig. 4. 1-dimensional powder pattern from an ettringite sample contained in a diamond anvil cell at ambient pressure together with a simulated pattern, calculated from a LeBail fit to our data, and a difference plot. Vertical tick marks show the predicted positions of diffraction peaks.
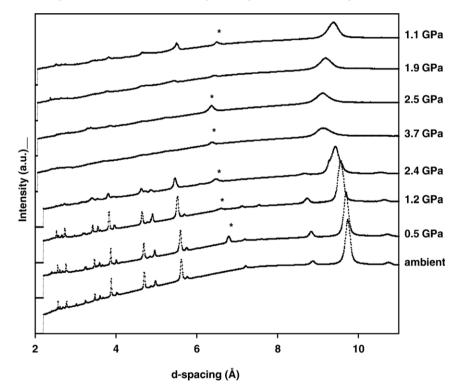

Fig. 5. Stack plot showing X-ray powder diffraction patterns collected from an ettringite sample at increasing pressures from ambient to 3.7 GPa and decreasing pressure from 3.7 to 1.1 GPa. The peak marked with an asterisk was unassigned but is not due to the sample.

stainless steel gasket (250 μm thickness, pre-indented to 70 μm) together with a ruby sphere for pressure determination [17,18]. In both runs a membrane diamond anvil cell equipped with 500 μm culet diamonds (1.6 mm height) and WC-backing plates was used. For the first run (10 pressure points) we used silicone oil as pressure medium whereas in the second run (4 pressure points) the

Table 2
Results of a LeBail fit to our data using the GSAS program

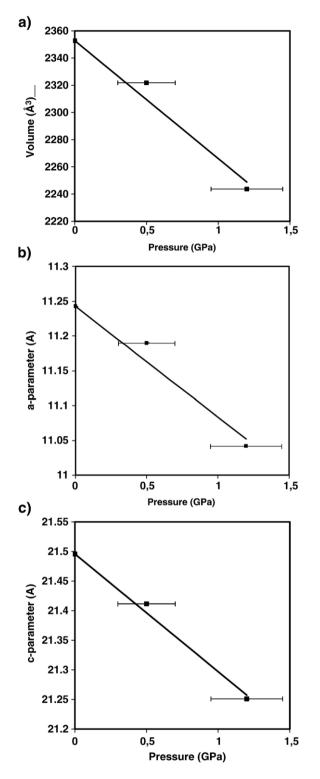| Pressure (GPa)	Volume (Å^3)	a (Å)	c (Å)	Background wRp	Background Rp	CHI^2
0.0001(0)	2352.8(1)	11.2422(4)	21.496(1)	0.0748	0.0484	0.8856
0.5(2)	2321.8(2)	11.1898(5)	21.411(2)	0.0233	0.016	0.1977
1.2(3)	2243.7(1)	11.0414(3)	21.251(1)	0.017	0.0107	0.04819

Fig. 6. Volume (a) and lattice parameters (b,c) determined for ettringite as a function of pressure. Linear fits to these data were used to estimate the isothermal bulk modulus and the two linear incompressibilities along the *a-* and *c*-directions.

sample was embedded in a 4:1 mixture of methanol:ethanol. In both runs diffraction patterns were collected while both increasing as well as decreasing pressure. Pressure was measured off-line using the ruby fluorescence method [17,18]. The 488 nm line of an Ar-ion laser was used to excite the fluorescence of the ruby crystal loaded into the gasket sample. The pressure dependent

fluorescence line was measured using a Roper Scientific spectrometer and analyzed using the WinView software supplied by Roper Scientific.

High-pressure infrared data were collected at beamline 1.4.3 of the advanced light source [19–21]. The infrared beam is collimated to about 10 μm in diameter. Spectra were collected using a Nicolet Magna 760 FTIR spectrometer with a resolution of 4 cm^{-1}. A special low profile diamond anvil cell suitable for use with the Nicolet spectrometer was used to generate high-pressures. The cell used 300 μm culets and type 2a diamonds [22]. Samples were contained in a 150 μm hole drilled into a stainless steel gasket. The gasket hole was first filled with KBr which had been dried for three days at 150 °C in a vacuum oven. The KBr sample was compressed between the diamonds to give a well packed gasket hole. A small amount of the KBr was then removed from the sample and one or two ruby chips were then packed into this small hole. Pressures were measured using the ruby fluorescence method. The ruby chips were placed close to the sample in order to minimize errors in pressure measurement. Prior to the acquisition of each sample spectrum a background spectrum was collected in an area of the KBr where there was no sample. Subsequently, a spectrum was collected from the sample from which the background spectrum was subtracted. Spectra were collected with increasing pressure from ambient to 6.4 GPa and then with decreasing pressure to ambient. A number of extra pressure cycles were performed to check the reproducibility of our results.

3. Results

An ambient pressure powder diffraction pattern from ettringite held in a diamond anvil cell is shown in Fig. 3. The shadow of the X-ray backstop is visible in the center of the pattern as well as the diffraction rings from the sample. All of our X-ray data were radially integrated to give two dimensional powder diffraction patterns using the fit2d program [23] using beam center, detector tilt and sample to detector distance determined using fit2d from a powder diffraction pattern from the NBS LaB$_6$ powder diffraction standard. The result of integrating the ambient pattern of Fig. 3 is shown in Fig. 4. All of the peaks can be identified as being due to the ettringite sample. The result of a weighted LeBail fit [24] to the ambient data using the Hartman and Berliner [8] structure as a starting point is shown in Fig. 4. The background was modeled with a shifted Chebeyshev function, peak profiles were fitted using a pseudo-Voigt function [25]. We obtained an adequate fit to our data which yielded lattice parameters of 11.2422(4) Å for *a* and 21.496(1) Å for *c* (where the number in parentheses is the 1σ uncertainty in the last digit) which compare well with the literature values of 11.26 Å and 21.48 Å [5,6] although they do deviate somewhat from the Hartman and Berliner values of 11.166881(82) Å and 21.35366 (22) Å [8]. The effect of pressure on the diffraction pattern of ettringite can be seen in Fig. 5 which contains a stack plot of the diffraction patterns collected using silicone oil as a pressure transmitting fluid. These patterns contain additional small peaks due to the pressure marker (corundum) and gasket scattering. The largest of these, at about 7 Å, is marked with an asterisk. On
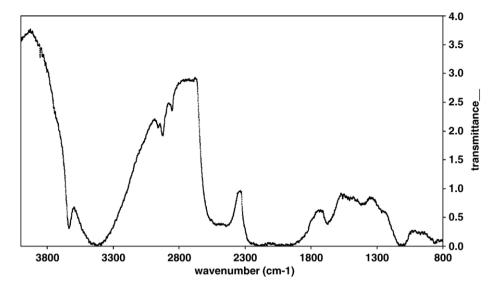
Fig. 7. Ambient infrared pattern collected from a sample of ettringite at ambient pressure in a diamond anvil cell. The strong absorption bands between 1800 and 2600 cm^{-1} are due to absorption by the diamonds.

increasing pressure to 1.2 GPa the diffraction peaks are seen to move to lower d-spacing, as the unit cell volume decreases, but the overall diffraction pattern does not show any significant change. At 2.4 GPa the peaks broaden and weaken and at 3.7 GPa are all gone except for a broad sample peak at about 9 Å and the original impurity peaks. On decreasing pressure the sample peaks are found to reappear. We were able to obtain satisfactory weighted LeBail fits to our 0.5 GPa and 1.2 GPa diffraction patterns (Table 2) but no satisfactory fit could be obtained with the subsequent patterns. An estimate of the bulk modulus of ettringite and incompressibility of the lattice parameters was made by linear fit to the pressure dependence of the unit cell volume and lattice parameters that we determined (Fig. 6). The isothermal bulk modulus of ettringite was found to be 27(7) GPa and the incompressibilities of the lattice parameters were found to be 71(30) GPa along the a-direction and 108(36) GPa along the c-direction. Data were also collected using a 4:1 methanol:ethanol mixture as a pressure transmitting medium instead of silicone oil in order to check if the sample environment has any effect on these transitions. The general behavior was found to be the same with the peaks broadening, disappearing and reappearing but the lattice parameters that we obtained differed markedly from those obtained in silicone oil. This may be due to the smaller methanol and ethanol molecules infiltrating the ettringite crystal lattice causing the individual lattice parameters to vary in an anomalous manner. Further work is required to fully understand this effect but this is out of the scope of the present study.

An infrared spectrum collected from an ettringite sample held in a diamond anvil cell at ambient pressure is shown in Fig. 7. Strong absorption lines from the diamonds are seen between 1800 and 2600 cm^{-1}. We assign the sharp absorption at 3634 cm^{-1} as being due to non-hydrogen bonded O–H stretch, the broad absorption at 3422 cm^{-1} as due to hydrogen bonded O–H stretch and free water, the peak at 1674 cm^{-1} as due to O–H bend and the peak at 1108 cm^{-1} as due to S–O stretch from SO_4^{2-} groups in line with previous assignments [26–29]. The effect of pressure on the infrared spectrum of ettringite is shown in Fig. 8. In the O–H stretch region (Fig. 8a) the non-hydrogen bonded O–H stretch absorbance is seen to decrease with increasing pressure and disappear at about 3 GPa. At the same time the broad hydrogen bonded absorption further broadens up to the maximum pressure of 6.4 GPa. On decreasing pressure the broad hydrogen bonded absorption is seen to sharpen and the non-hydrogen bonded absorption reappears to give a spectrum that is very similar to the original ambient spectrum. In the low frequency section of the spectra (Fig. 8b) we see the O–H stretch band broaden with pressure and sharpen on pressure release while the sulfate band does not change in width or intensity but moves to lower frequency on pressurization and higher frequency on pressure release. The position of the sulfate band as a function of pressure is shown in Fig. 9. The band is seen to linearly increase in frequency at a rate of about 12 cm^{-1}/GPa until about 3 GPa when it then linearly increases at a rate of about 5.9 cm^{-1}/GPa.

4. Discussion

Both the infrared and diffraction data show a transformation in ettringite at about 3 GPa. The X-ray data show the structure of ettringite transforming to a distorted version of the ambient crystal structure and then losing long range order as the pressure is increased ending up with only a broad basal reflection. We interpret this as being due to strain on the crystal structure inducing increasing amounts of disorder leading to amorphization. The return of X-ray diffraction peaks indicates that the crystalline to amorphous transition is reversible. Our data indicate that this is a continuous transition but further data collection with a finer pressure sampling is required to confirm this. The infrared data give us some indication of the mechanism of this amorphization. We see a decrease in the number of hydroxyl groups that are non-hydrogen bonded and an increase in the width of the hydrogen bonded O–H stretch peak. This we
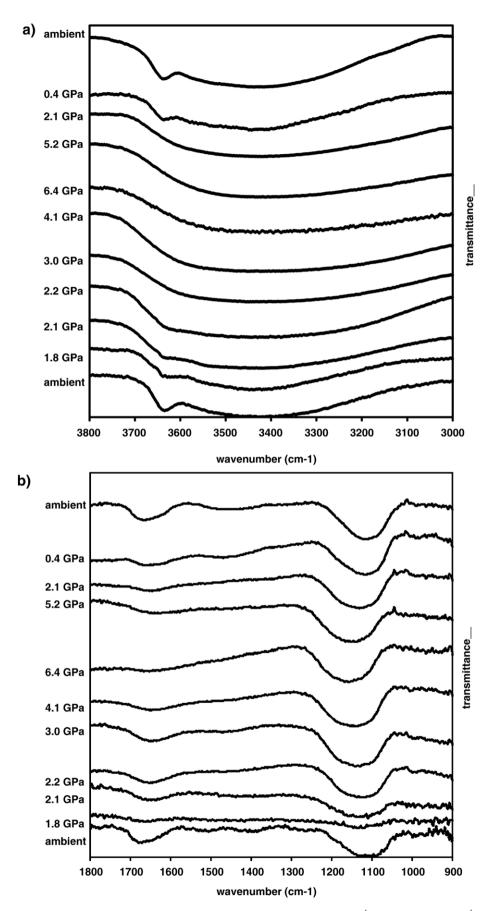
Fig. 8. Variation of the infrared absorbance as a function of pressure in the 3000–3800 cm^{-1} (a) and 900–1800 cm^{-1} (b) ranges.
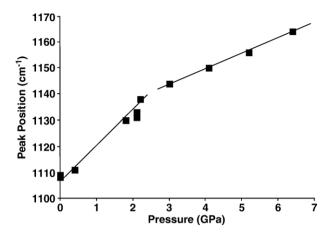
Fig. 9. Variation of the sulfate infrared absorption band of ettringite as a function of pressure.

interpret as being due to an increased number of hydroxyl bonding environments as the crystal structure becomes more disordered. The sulfate S–O stretch band moves to higher frequency with increasing pressure which we interpret as being due to bond shortening but remains intact throughout the amorphization and re-crystallization. We interpret this as indicating that the basic structural units within the crystal structure remain intact but disorder with respect to each other and the free water in the structure. We can not tell if the amorphization is associated with dehydration of the structure as happens during thermal decomposition [14] but the prevalence of the hydroxyl bands and the reversibility of the transitions suggest that no dehydration occurs. $Ca(OH)_2$ [30], $Ni(OH)_2$ and $Co(OH)_2$ [31] all exhibit a reversible pressure induced amorphization near 11 GPa. These amorphizations have been found to be caused by disruption of the network of hydrogen bonds [32]. This may also be the case for ettringite.

Acknowledgements

References

[1] H.F.W. Taylor, Cement Chemistry, Thomas Telford, London, 1997.
[2] M. Santhanam, M.D. Cohen, J. Olek, Sulfate attack research – whither now? Cement and Concrete Research 31 (2001) 845–851.
[3] H.F.W. Taylor, C. Famy, K.L. Scrivener, Delayed ettringite formation, Cement and Concrete Research 31 (2001) 683–693.
[4] P.K. Mehta, P.J.M. Montiero, Concrete: Microstructure, Properties and Materials, third edition. McGraw-Hill, 2006.
[5] A.E. Moore, H.F.W. Taylor, Crystal structure of ettringite, Nature 218 (1968) 1048–1049.
[6] A.E. Moore, H.F.W. Taylor, Crystal structure of ettringite, Acta Crystallographica B26 (1970) 386–393.
[7] R. Berliner, in: M. Cohen, S. Mindness, J. Skalny (Eds.), The Structure of Ettringite, Materials Science of Concrete – The Sydney Diamond Symposium, 1998, pp. 127–141.
[8] M.R. Hartman, R. Berliner, Investigation of the structure of ettringite by time-of-flight neutron powder diffraction techniques, Cement and Concrete Research 36 (2006) 364–370.
[9] S.J. Barnett, C.D. Adams, A.R.W. Jackson, Solid solution between ettringite $Ca_6Al_2(SO_4)_3(OH)_{12}.26H_2O$ and thaumasite $Ca_3SiSO_4CO_3(OH)_6.12H_2O$, Journal of Materials Science 35 (2000) 4109–4114.
[10] G.J. McCarthy, D.J. Hassett, J.A. Bender, Synthesis, crystal structure and stability of ettringite, a material with potential applications in hazardous waste immobilization, Advanced Cementitious Systems: Mechanisms and Properties, Materials Research Society Symposium Proceedings Series, vol. 245, 1992, pp. 129–140.
[11] Y. Shimada, J.F. Young, Structural changes during thermal dehydration of ettringite, Advances in Cement Research 13 (2001) 77–81.
[12] N.N. Skoblinskaya, K.G. Krasilnikov, Changes in crystal structure of ettringite on dehydration 1, Cement and Concrete Research 5 (1975) 381–394.
[13] N.N. Skoblinskaya, K.G. Krasilnikov, L.V. Nikitina, V.P. Varlamov, Changes in crystal structure of ettringite on dehydration 2, Cement and Concrete Research 5 (1975) 419–432.
[14] M.R. Hartman, S.K. Brady, R. Berliner, M.S. Conradi, The evolution of structural changes in ettringite during thermal decomposition, Journal of Solid State Chemistry 179 (2006) 1259–1272.
[15] B. Cairncross, N.J. Beukes, J. Gutzmer, The Manganese Adventure: The South African Manganese Field, Associated Ore and Metal Corporation, Johannesburg, 1997, p. 236.
[16] M. Kunz, A.A. MacDowell, W.A. Caldwell, D. Cambie, R.S. Celestre, E.E. Domning, R.M. Duarte, A.E. Gleason, J.M. Glossinger, N. Kelez, D.W. Plate, T. Yu, J.M. Zaug, H.A. Padmore, R. Jeanloz, A.P. Alivisatos, S.M. Clark, A beamline for high pressure studies at the Advanced Light Source with a superconducting bending magnet as the source, Journal of Synchrotron Radiation 12 (5) (2005) 650–658.
[17] H.-K. Mao, J. Xu, P.M. Bell, Journal of Geophysical research – Solid Earth and Planets 91 (B5) (1986) 4673–4676.
[18] G.J. Piermarini, S. Block, J.D. Barnett, R.A. Forman, Journal of Applied Physics 46 (6) (1995) 2774–2780.
[19] W.R. McKinney, C.J. Hirschmugl, H.A. Padmore, T. Lauritzen, N. Andresen, G. Andronaco, R. Patton, M. Fong, The first infrared beamline at the ALS: design, construction, and commissioning, SPIE Proceedings 3153 (1997) 59–76.
[20] M.C. Martin, W.R. McKinney, The first synchrotron infrared beamlines at the advanced light source: microspectroscopy and fast timing, Proc. Mater. Res. Soc., vol. 524, 1998, p. 11.
[21] W.R. McKinney, M.C. Martin, J. Byrd, R. Miller, M. Chin, G. Portman, E.J. Moler, T. Lauritzen, J.P. McKean, M. West, N. Kellogg, V. Zhuang, P.N. Ross, J.W. Ager III, W. Shan, E.E. Haller, The first infrared beamlines at the ALS: final commissioning and new end stations, SPIE Proceedings 3775 (1999) 37–43.
[22] B.R. Angel, M.J.A. Smith, J.J. Charette, Correlation between the nitrogen impurity content and the crystal habit of synthetic diamond, Nature 218 (1968) 1246–1247.
[23] A.P. Hammersley, S.O. Svensson, M. Hanfland, A.N. Fitch, D. Hausermann, Two-dimensional detector software: from real detector to idealized image or two-theta scan, High Pressure Research 14 (1996) 235–248.
[24] A. LeBail, Extracting structure factors from powder diffraction data by iterating full pattern profile fitting, in: E. Prince, J.K. Stalick (Eds.), Accuracy in Powder Diffraction II, Special Publication, vol. 846, NIST, Gaithersburg, MD, 1992, p. 213.
[25] B.H. Toby, EXPGUI, a graphical user interface for GSAS, Journal of Applied Crystallography 34 (2001) 210–213.
[26] S.J. Barnett, D.E. Macphee, E.E. Lachowski, N.J. Crammond, XRD, EDX and IR analysis of solid solutions between thaumasite and ettringite, Cement and Concrete Research 32 (2002) 719–730.
[27] S.C.B. Myneni, S.J. Traina, G.A. Waychunas, T.J. Logan, Vibrational spectroscopy of functional group chemistry and arsenate coordination in ettringite, Geochimica et Cosmochimica Acta 62 (1998) 3499–3514.

[28] M.Y.A. Mollah, F. Lu, D.L. Cocke, An X-ray diffraction and Fourier transform infrared spectroscopic characterization of the speciation of arsenic (V) in Portland cement type-V, The Science of the Total Environment 224 (1998) 57–68.

[29] M.A. Trezza, A.E. Lavat, Cement and Concrete Ressearch 31 (2001) 869–872.

[30] C. Meade, R. Jeanloz, Geophysical Research Letters 17 (1990) 1157–1160.

[31] J.H. Nguyen, M.B. Kruger, R. Jeanloz, Physical Review B 49 (1994) 3734–3738.

[32] T.S. Duffy, R.J. Hemley, H.-K. Mao, Deep Earth and Planetary Volatiles, AIP, New York, 1994.